Decolorization of C.I. Acid Blue 9 solution by UV/Nano-TiO$_2$, Fenton, Fenton-like, electro-Fenton and electrocoagulation processes: A comparative study

A.R. Khataee*, V. Vatanpour, A.R. Amani Ghadim

Water and Wastewater Treatment Research Laboratory, Department of Applied Chemistry, Faculty of Chemistry, University of Tabriz, Tabriz, Iran

ARTICLE INFO

ABSTRACT

This study makes a comparison between UV/Nano-TiO$_2$, Fenton, Fenton-like, electro-Fenton (EF) and electrocoagulation (EC) treatment methods to investigate the removal of C.I. Acid Blue 9 (AB9), which was chosen as the model organic contaminant. Results indicated that the decolorization efficiency was in order of Fenton > EC > UV/Nano-TiO$_2$ > Fenton-like > EF. Desired concentrations of Fe^{2+} and H$_2$O$_2$ for the abatement of AB9 in the Fenton-based processes were found to be 10^{-4} M and 2×10^{-3} M, respectively. In the case of UV/Nano-TiO$_2$ process, we have studied the influence of the basic photocatalytic parameters such as the irradiation time, pH of the solution and amount of TiO$_2$ nanoparticles on the photocatalytic decolorization efficiency of AB9. Accordingly, it could be stated that the complete removal of color, after selecting desired operational parameters could be achieved in a relatively short time, about 25 min. Our results also revealed that the most effective decomposition of AB9 was observed with 150 mg/l of TiO$_2$ nanoparticles in acidic condition. The effect of operational parameters including current density, initial pH and time of electrolysis were studied in electrocoagulation process. The results indicated that for a solution of 20 mg/l AB9, almost 98% color were removed, when the pH was about 6, the time of electrolysis was 8 min and the current density was approximately 25 A/m^2 in electrocoagulation process.
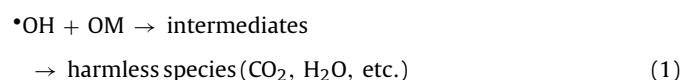
© 2008 Elsevier B.V. All rights reserved.

1. Introduction

Presence of color and its causative compounds has always been undesirable in water used for either industrial or domestic needs. Different coloring agents like dyes, inorganic pigments, tannins, lignins, etc. usually impart color. Among complex industrial wastewater with various types of coloring agents, dye wastes are predominant [1,2]. Dyes present in wastewater are of particular environmental concern since they not only give an undesirable color to the waters but also in some cases are themselves harmful compounds and can originate dangerous by-products through oxidation, hydrolysis, or other chemical reactions taking place in the waste phase [3]. Thus, there is an urgent need for textile industries to develop effective methods of water processing.

Commonly applied treatment methods for color removal from dye-contaminated effluents consist of various processes involving biological, physical and chemical decolorization methods [4]. Conventional treatments of dye effluents include biological oxidation and adsorption. Although less expensive than other approaches, biological treatment is ineffective for decolorization because the dyes are toxic. Adsorption onto activated carbon transfers most of the contaminant from the wastewater to the solid phase. This method therefore requires further disposal of the sludge.

In recent years, advanced oxidation processes (AOPs) and electrochemical methods have been developed to treat the contaminants of drinking water and industrial effluents. Advanced oxidation processes almost all are based on the generation of reactive species such as hydroxyl radicals ($^{\bullet}$OH) which degrade a broad range of organic pollutants quickly and non-selectively. Although it is claimed that there are other species involved, the active species responsible for the destruction of contaminants in most cases seems to be the hydroxyl radical ($^{\bullet}$OH) which is unstable and quite reactive. Due to the instability of $^{\bullet}$OH radical, it must be generated continuously "in situ" through chemical or photochemical reactions [5]. The organic matters (OMs) in the solution are attacked by hydroxyl radical as soon as $^{\bullet}$OH is generated, as described in the following equation:

$$^{\bullet}\text{OH} + \text{OM} \rightarrow \text{intermediates}$$
$$\rightarrow \text{harmless species} (\text{CO}_2, \text{H}_2\text{O}, \text{etc.}) \tag{1}$$

The important advanced oxidation processes are H$_2$O$_2$/Fe^{2+} (Fenton's reagent) [6], H$_2$O$_2$/Fe^{3+} (Fenton-like reagent) [7], electro-Fenton [8] and H$_2$O$_2$/O$_3$ [9] as chemical procedures, UV/H$_2$O$_2$/Fe^{2+},
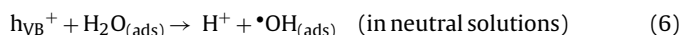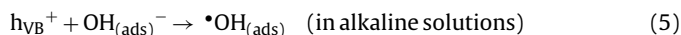
* Corresponding author. Tel.: +98 411 3393165; fax: +98 411 3340191.
E-mail addresses: a_khataee@tabrizu.ac.ir (A.R. Khataee),
vahidvatanpour@yahoo.com (V. Vatanpour),
a.r_amani@yahoo.com (A.R. Amani Ghadim).

UV/H_2O_2/Fe^{3+} [10,11], UV/H_2O_2 [12], UV/O_3 [13] and photoelectro-Fenton [14] as photoelectrochemical treatment, and UV/TiO_2 [15,16], UV/TiO_2/O_3 [17] and UV/ZnO [18,19] as photocatalytic methods. The versatility of AOP is also enhanced by the fact that they offer different possible ways for hydroxyl radical's production thus allowing a better compliance with the specific treatment requirements.

Among them, heterogeneous photocatalysis using TiO_2 or ZnO nanoparticles is regarded as a promising method for the transformation of toxic and bioresistant compounds into harmless species (CO_2, H_2O, etc.). With the advent of nanotechnology the nanostructured TiO_2 has found a great deal of applications. Nanotechnology is a growing and cutting edge technology with applications in many fields of research and development areas including biology, chemistry, material science, medicine and physics. With the inception of nanoscience and nanotechnology nanoscale materials, in general, and nanostructured TiO_2 materials, in particular, have received significant attention. With a typical dimension of less than 100 nm, nanostructured TiO_2 materials have become attractive for numerous applications in different fields. It is known to have golden properties, which include non-toxicity, abundance, and potentially least costly compared to other nanomaterials [20,21]. Briefly, TiO_2 is a semiconductor and when it is illuminated with the light of $\lambda < 390$ nm, electrons are promoted from the valence band to the conduction band of the semiconducting oxide to give electron–hole pairs [15,22,23]:

$$TiO_2 + h\nu \, (\lambda < \, 390 \, nm) \rightarrow \, e^- + h^+ \tag{2}$$
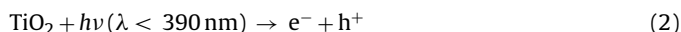
The valence band (h^+) potential is positive enough to generate hydroxyl radicals at the surface of TiO_2 and the conduction band (e^-) potential is negative enough to reduce molecular oxygen as shown in the following equations:

$$e^- + O_{2(ads)} \rightarrow \, ^\bullet O_{2(ads)}{}^- \tag{3}$$

$$e^- + H_{(ads)}{}^+ \rightarrow \, ^\bullet H_{(ads)} \tag{4}$$

$$h_{VB}{}^+ + OH_{(ads)}{}^- \rightarrow \, ^\bullet OH_{(ads)} \quad \text{(in alkaline solutions)} \tag{5}$$

$$h_{VB}{}^+ + H_2O_{(ads)} \rightarrow \, H^+ + {}^\bullet OH_{(ads)} \quad \text{(in neutral solutions)} \tag{6}$$

The hydroxyl radical is a powerful oxidizing agent and attacks organic matters present at or near the surface of TiO_2. It causes, ultimately, complete decomposition of toxic and bioresistant compounds into harmless species (CO_2, H_2O, etc.) [22,24].

The other advanced oxidation processes are Fenton-based processes. Fenton's reagent is a mixture of ferrous ion (Fe^{2+}) and hydrogen peroxide (H_2O_2) generating hydroxyl radical ($^\bullet OH$) in situ according to the following equation:

$$Fe^{2+} + H_2O_2 \rightarrow \, Fe^{3+} + OH^- + {}^\bullet OH \tag{7}$$

Fe(III) can catalyze the decomposition of H_2O_2. The reaction of H_2O_2 with Fe(III) (so called the Fenton's-like reagent) goes through the formation of hydroperoxyl radical $HO_2{}^\bullet$ [25]:

$$Fe^{3+} + H_2O_2 \rightarrow \, Fe^{2+} + HO_2{}^\bullet + H^+ \tag{8}$$
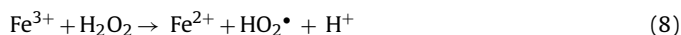
In electro-Fenton method, $^\bullet OH$ radicals are produced in the bulk of the solution from the reaction of electrogenerated H_2O_2 and Fe^{2+} (Eq. (7)). Hydrogen peroxide is produced electrochemically upon two electron reduction of oxygen on several electrodes (mercury pool, graphite, carbon polytetrafluoroethylene O_2-fed cathodes) [26,27] according to the following equation:
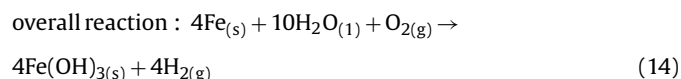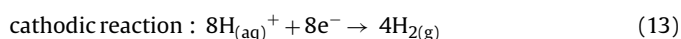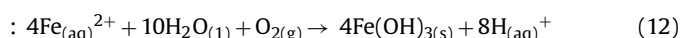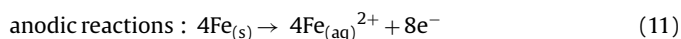
$$O_2 + 2e^- + 2H^+ \rightarrow \, H_2O_2 \tag{9}$$

In this system, catalytic reaction can be propagated via Fe^{2+} regeneration which mainly takes place by the reduction of Fe^{3+}

species with electrogenerated H_2O_2 (Eq. (8)) and reduction of it in cathode surface (Eq. (10)):

$$Fe^{3+} + e^- \rightarrow \, Fe^{2+} \tag{10}$$

This system has been used successfully for the decolorization of different organic dyes [28,29].

Electrocoagulation (EC) is an alternative approach which was widely used in wastewater treatment loaded from textile industries [30,31]. This process includes the generation of coagulants in situ by dissolving electrically either aluminium or iron ions in aluminium or iron electrodes, respectively. The metal ions generation takes place at the anode and the hydrogen gas is released from the cathode. The hydrogen gas would also help float the flocculated particles out of water. When a potential is applied from an external power source, the anode material undergoes oxidation, while the cathode will be subjected to reduction of water [32]. Electrocoagulation of wastewater using iron electrodes takes place according to the following reactions:

$$\text{anodic reactions}: 4Fe_{(s)} \rightarrow \, 4Fe_{(aq)}{}^{2+} + 8e^- \tag{11}$$

$$: 4Fe_{(aq)}{}^{2+} + 10H_2O_{(1)} + O_{2(g)} \rightarrow \, 4Fe(OH)_{3(s)} + 8H_{(aq)}{}^+ \tag{12}$$

$$\text{cathodic reaction}: 8H_{(aq)}{}^+ + 8e^- \rightarrow \, 4H_{2(g)} \tag{13}$$

$$\text{overall reaction}: 4Fe_{(s)} + 10H_2O_{(1)} + O_{2(g)} \rightarrow$$
$$4Fe(OH)_{3(s)} + 4H_{2(g)} \tag{14}$$

The generated $Fe_{(aq)}{}^{3+}$ ions will immediately undergo further spontaneous reactions to produce corresponding hydroxides and/or polyhydroxides. These hydroxides/polyhydroxides/polyhydroxymetallic compounds have strong affinity with dispersed/dissolved as well as the counter ions to cause coagulation/adsorption [33–35].

C.I. Acid Blue 9 (AB9) which belongs to acidic dyes group is soluble in cold water and methanol. It can be found in thousands of textile (as a dye for wool and silk), foodstuff and pharmaceutical wastewaters. In addition, C.I. Acid Blue 9 is one of the components Aquashade which can be used as an aquatic algaecide/herbicide, in natural or manmade ponds, lakes, fountains, fish farms, and fish hatcheries, and may be applied by both professional applicators and homeowners. It is hazardous in case of ingestion, of skin contact (irritant), of eye contact (irritant), of inhalation [36].
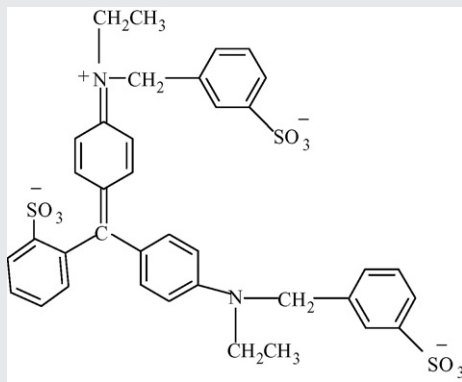
In the present research work various advanced oxidation processes and electrochemical methods including UV/Nano-TiO_2, Fenton, Fenton-like, electro-Fenton and electrocoagulation processes were applied to decolorization of the solution containing C.I. Acid Blue 9. In each process the most effective operational parameters were investigated. Moreover, the performance of these processes in terms of decolorization efficiency, kinetic rate constant and electrical energy consumption was compared.

2. Materials and methods

2.1. Chemicals

TiO_2 Degussa P-25 nanoparticles (having 80% anatase and 20% rutile, specific surface area (BET) 50 m^2/g and particle size 21 nm) were kindly supplied by Degussa Co., Germany. To determine the crystal phase composition of TiO_2 nanoparticles, X-ray diffraction (XRD) measurements were carried out at room temperature by using Siemens X-ray diffraction D5000 with Cu Kα radiation ($\lambda = 0.15478$ nm). The accelerating voltage of 40 kV and emission

Table 1
Structure and characteristics of C.I. Acid Blue 9

Structure	
Chemical class	Triphenyl methane
Color index number	42,090
λ_{max} (nm)	625 (406)
M_w (g mol^{-1})	792.86

current of 30 mA were used. The average crystalline size of the samples was calculated according to Debye–Scherrer formula:

$$D = \frac{0.9\lambda}{\beta\cos\theta} \tag{15}$$

where D is the average crystallite size (Å), λ is the wavelength of the X-ray radiation (Cu Kα = 1.54178 Å), β is the full width at half maximum (fwhm) intensity of the peak and θ is the diffraction angle. The mean particle size of Degussa P-25 sample was calculated about 21 nm. C.I. Acid Blue 9 was obtained from Shimi Keshavarz Company, Iran. Its structure and characteristics is given in Table 1. The chemicals including HClO$_4$ (70%), HNO$_3$ (65%), NaClO$_4$·H$_2$O, FeSO$_4$·2H$_2$O, H$_2$O$_2$ (30%), H$_2$SO$_4$, NaOH and Fe(NO$_3$)$_3$·9H$_2$O were obtained from Merck.

2.2. UV/Nano-TiO$_2$ process

For the UV/Nano-TiO$_2$ process, irradiation was carried out with a 30-W (UV-C) mercury lamp (Philips), which was put above a batch photoreactor of 500 ml volume. The wavelength of the emitted light (lamp) was 254 nm. The distance between solution and UV source was constant, 15 cm, in all experiments. The light intensity of UV lamp at the surface of the solution was 11.2 W m^{-2}. The desired concentration of C.I. Acid Blue 9 (20 mg/l) and TiO$_2$ nanoparticles were fed into the Pyrex reactor. The TiO$_2$ suspension is sonicated for 10 min before illumination to disperse TiO$_2$ nanoparticles uniformly in the solution by sonoplus ultrasonic homogenizer HD 2200, Germany. The pH of the solution was adjusted using dilute sulphuric acid and aqueous sodium hydroxide solutions and measured by pH meter (Philips PW 9422). Then, the UV lamp was switched on to initiate the reaction. The thickness of the solution in the photoreactor was 19 mm. During irradiation, agitation was maintained to keep the suspension homogeneous. At regular time intervals, samples were taken and the remaining AB9 was analyzed. In order to remove the TiO$_2$ particles the samples were centrifuged and filtered.

2.3. Electro-Fenton process

Electrolyses were performed with a dc power supply. The cell voltage was determined with a UNI-T (UT2002) digital multimeter. The electro-Fenton experiments were conducted at room temperature in an open, undivided and cylindrical glass cell of 500 ml capacity and performed at constant potential. The commercial graphite felt (thickness = 0.4 cm) with 9.5 cm^2 surface area was selected as cathode. The Pt sheet of 1 cm^2 area was used as anode and the reference electrode was a saturated calomel electrode (SCE). In all experiments, solutions were stirred magnetically at a rate of 200 rpm. Prior to the electrolysis, O$_2$ was bubbled for 10 min through the solution. During electrolysis, O$_2$ was sparged by rate of 20 ml/min. Samples (200 ml) containing dye in 0.05 M NaClO$_4$ electrolyte were degraded at constant potentials of −0.5 V. The used conditions for this work were optimized in previous work [37].

2.4. Fenton and Fenton-like processes

Fenton and Fenton-like batch experiments were performed in beakers with a reaction mixture of dye, Fe^{2+} or Fe^{3+} and H$_2$O$_2$. The required amounts of iron ions were added and the pH was adjusted in optimum amount of 3.0 with sulphuric acid. With addition of H$_2$O$_2$, Fenton reaction is initiated. Continuous mixing was provided by a magnetic stirrer.

2.5. Electrocoagulation process

All electrocoagulation experiments were performed in batch electrolyte cell. The volume of cell was 500 ml. Iron (ST 37-2) plates were used as anode, and steel (grade 304) plates were used as cathode. Dimensions of electrodes were 40 mm × 50 mm × 1 mm and the distance between two electrodes was 15 mm in all experiments. The electrodes were connected to a dc power supply (ADAK PS808, Iran) with galvanostatic operational options for controlling the current density (CD). In each run, 200 ml of AB9 solution was placed into the electrolytic cell. The conductivity measurement was carried out using a Philips conductivity meter (PW 9509, England). The operation started when the current density was adjusted to a desired value. During process, the solution was agitated at 200 rpm to form and float the flocs. At the end of EC, the solution was filtered through 0.2 μm membrane filter (Schliecher & Schuell, Germany) and then the samples were analyzed.

2.6. Analytical procedure

In all of the above-mentioned processes, at regular time intervals, samples were taken and the remaining AB9 was determined using a Lightwave S2000 UV/vis spectrophotometer at λ_{max} = 625 nm and calibration curve. Using this method, the color removal efficiency (R) of AB9 could be obtained at different intervals.

3. Results and discussion

3.1. Decolorization efficiency of UV/Nano-TiO$_2$ process

The efficiency of photocatalytic processes strongly depended upon the pH of the reaction solution. This is due to the amphoteric behavior of semiconducting titanium dioxide. The surface charge properties of TiO$_2$ change with the changes of pH values [36]. Fig. 1 demonstrates the photodegradation of AB9 at different pH from 2 to 12. As it is clear from the figure, the best results were obtained in acidic condition. According to the zero point of charge of TiO$_2$, its surface is presumably positively charged in acidic solution and negatively charged in alkaline solution [38,39]. Since AB9 has a sulphuric group in its structure, which is negatively charged, the acidic solution favors adsorption of it onto photocatalyst surface, thus the photodegradation efficiency increases. There is also the photocatalytic degradation of AB9 in acidic solutions, which is probably due
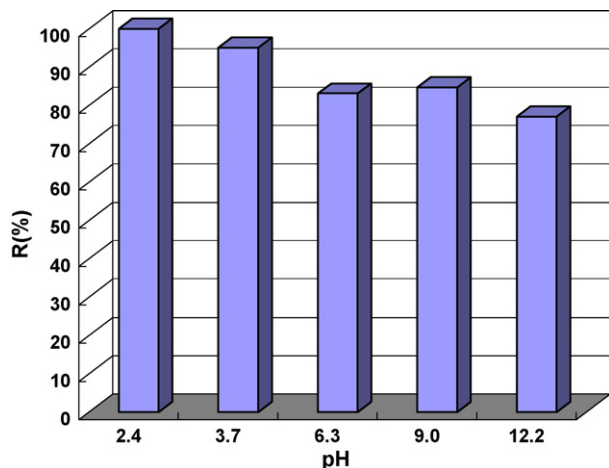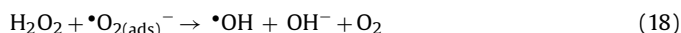
Fig. 1. Effect of pH on photodegradation efficiency of AB9 at the irradiation time of 15 min; $C_0 = 20$ mg/l, $[TiO_2]_0 = 150$ mg/l, and stirring speed = 200 rpm.

Fig. 3. UV–vis spectra changes of AB9 (20 mg/l) in aqueous TiO_2 P-25 dispersion (TiO_2 150 mg/l) irradiated with a mercury lamp light at pH 6.3, at various irradiation times.

to the formation of $^\bullet OH$ as it can be inferred from the following reactions (Eqs. (3) and (16)–(18)) [15]:

$$^\bullet O_{2(ads)}^- + H^+ \rightarrow HO_2^\bullet \qquad (16)$$

$$2HO_2^\bullet \rightarrow O_2 + H_2O_2 \qquad (17)$$

$$H_2O_2 + {}^\bullet O_{2(ads)}^- \rightarrow {}^\bullet OH + OH^- + O_2 \qquad (18)$$

Experiments performed with different concentrations of TiO_2 nanoparticles (Fig. 2) showed that the photodegradation efficiency increased with an increase in the amount of nanophotocatalyst but once it exceeded a certain level (150 mg/l), it was accompanied by a decrease in photodegradation efficiency. The most effective decomposition of AB9 was observed with 150 mg/l of TiO_2 nanoparticles. Increasing the concentration of the photocatalyst gave rise to a higher number and density of TiO_2 nanoparticles, which in turn caused photons absorbed and AB9 molecules adsorbed to increase. All of these processes went hand in hand to enhance the efficiency of photodegradation. Above a certain level (150 mg/l), the substrate molecules available were not sufficient for adsorption by the increased number of TiO_2 particles. Hence the additional catalyst powder was not involved in the catalyst's activity and the photodegradation efficiency did not increase with an increase in the amount of catalyst beyond a certain limit. Another cause for this is supposedly an increased opacity of the suspension, brought about as a result of excess of TiO_2 particles [40,41].

Fig. 3 shows a typical time-dependent UV–vis spectrum of AB9 solution during photocatalytic process. The spectrum of AB9 in the visible region exhibits a main band with a maximum at 625 nm. As it
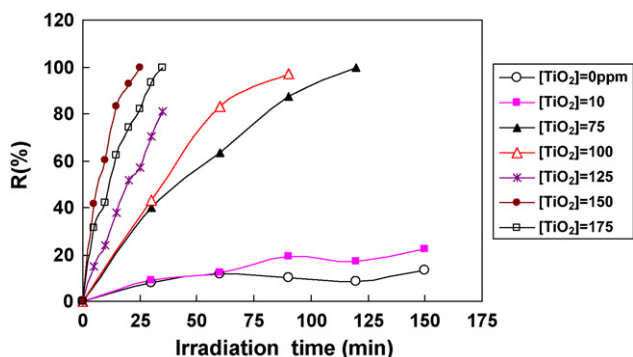

Fig. 2. Effect of the amount of TiO_2 nanoparticles on photodegradation efficiency of AB9; $C_0 = 20$ mg/l, pH 6.3, and stirring speed = 200 rpm.
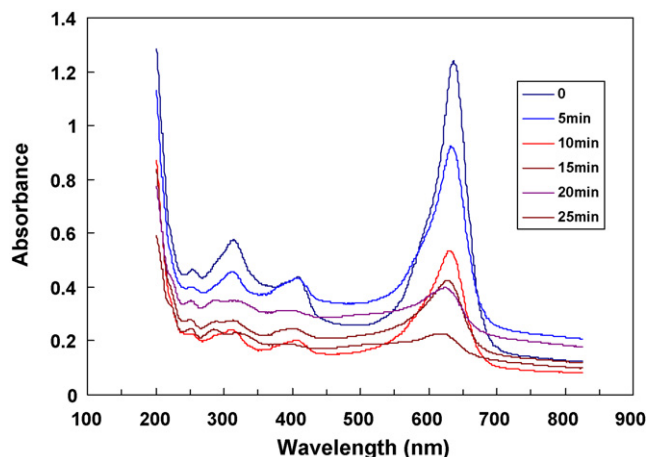
is clear from this figure, the absorption peaks diminished and finally disappeared under reaction, which indicated that the AB9 had been degraded. No new absorption bands appear in either the visible or ultraviolet regions. Complete removal of AB9 was observed after 25 min in the desired conditions.

3.2. Decolorization efficiency of Fenton and Fenton-like processes

To determine the desired conditions of Fenton and Fenton-like processes for the decolorization of AB9 dye, important variables such as effect dosage of H_2O_2 and iron ion concentration on color removal efficiency was investigated. In order to investigate the effect of H_2O_2 concentration on the decolorization efficiency, experiments were conducted at different H_2O_2 concentrations with 10^{-4} M Fe^{2+} or Fe^{3+} solutions. Fig. 4a and b shows the relationship between the decolorization of dye and the initial concentration of H_2O_2 in the Fenton and Fenton-like processes. To render the Fenton and Fenton-like processes competitive with other processes, it is essential that their applications represent a low cost operation, which basically implies a better control of H_2O_2 dosage. The objective of this evaluation is to select the effective operational concentration of H_2O_2 in Fenton and Fenton-like processes. For the Fenton process, the addition of H_2O_2 from 4×10^{-4} M to 2×10^{-3} M increases the decolorization of the dye from 86% to 96% at 10 min. The increase in the decolorization is due to the increase in hydroxyl radical concentration by addition of H_2O_2. Further increase from 2×10^{-3} M to 3×10^{-3} M causes little decrease in decolorization. This little increase is due to the fact that at a higher H_2O_2 concentration scavenging of hydroxyl radicals will occur, which can be expressed by the following equations [42]:

$$HO^\bullet + H_2O_2 \rightarrow H_2O + HO_2^\bullet \qquad (19)$$

$$HO_2^\bullet + HO^\bullet \rightarrow H_2O + O_2 \qquad (20)$$

In the Fenton-like process, the addition of H_2O_2 between 4×10^{-4} M and 2×10^{-3} M increases decolorization from 50% to 94%, respectively at 70 min. Further increase causes no significant change in decolorization for Fenton-like processes.

Fig. 5a and b shows the effect of iron ion concentration on the dye degradation in Fenton and Fenton-like reactions. The extent of degradation of the dye increased with increasing iron ion concentration. In the case of Fenton oxidation, an obvious increase of the decolorization efficiency was observed by raising initial Fe^{2+} concentration from 5×10^{-5} M to 10^{-4} M. However, further increase
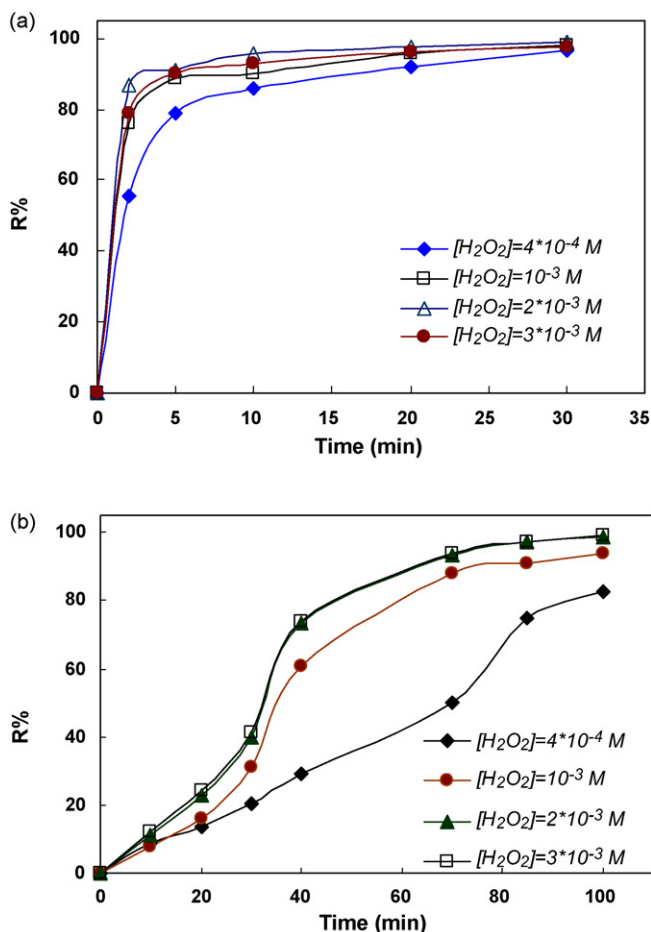
Fig. 4. Effect of H_2O_2 concentration on AB9 decolorization; pH 3.0, $C_0 = 20$ mg/l, and stirring speed = 200 rpm. (a) Fenton process: $[Fe^{2+}] = 10^{-4}$ M; (b) Fenton-like process: $[Fe^{3+}] = 10^{-4}$ M.

Fig. 5. Effect of iron ion concentration on AB9 decolorization; pH 3.0, $C_0 = 20$ mg/l, and stirring speed = 200 rpm. (a) Fenton process (Fe^{2+}, after 10 min); (b) Fenton-like process (Fe^{3+}, after 70 min).

in the concentration of ferrous ions above 10^{-4} M did not brought about further improvement in the dye removal. This fact was probably due to the consumption of the percentage of $^\bullet$OH by an excess of ferrous ions (Eq. (21)) [27]:

$$Fe^{2+} + {}^\bullet OH \rightarrow Fe^{3+} + OH^- \qquad (21)$$

For Fenton-like process, when the iron ion concentration was 5×10^{-5} M, dye removal was only 71% after 70 min. By contrast, the extent of degradation was 91%, 93% and 97% after 70 min at Fe^{3+} concentration of 10^{-4} M, 2×10^{-4} M and 3×10^{-4} M, respectively.

Fig. 6a and b shows the effect of ratio of $[H_2O_2]/[Fe$ ion] on AB9 decolorization, in Fenton and Fenton-like reactions. In the case of Fenton oxidation, with increasing of ratio from 4 to 20 decolorization efficiency was increased. However, further increase did not cause to further removal. In the case of Fenton-like, with increasing of ratio from 20 removal did not reduce and decolorization efficiency did not considerably increase.

3.3. Decolorization efficiency of electro-Fenton process

The pH of solution in the electro-Fenton process has important influence in H_2O_2 electrogeneration and stability of iron ions. In this order, effect of pH on color removal efficiency of AB9 was investigated. Fig. 7 shows the comparative decolorization of 200 ml solutions containing 20 mg/l of AB9 at different pH under −0.50 V/SCE constant cathodic potential. As it can be seen, the best
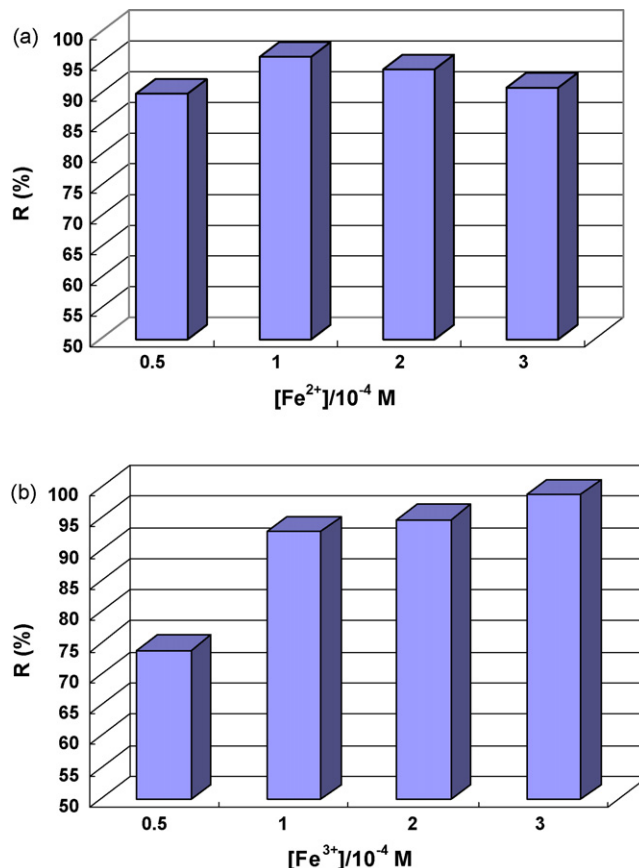
pH is 3.0. Decolorization efficiency decreased from 90% to 38% at 120 min with increasing pH from 3.0 to 5.0. Results show that below pH 3.0 color removal efficiency is decreased due to enhanced hydrogen evaluation on the cathode surface [43]. On the other hand, high concentration of H^+ ions inhibit the formation of $Fe-OOH^{2+}$ complex from reaction of Fe^{3+} and H_2O_2 [7]. At pH above 3.0 due to insufficient protons concentration for H_2O_2 electrogeneration [43] and also precipitation of Fe(III) [44], decolorization efficiency is reduced.

In order to investigate the effect of initial ferric concentration on the decolorization efficiency of AB9, several electrolyses of 200 ml containing 20 mg/l AB9 with initial pH 3.0 were carried out at −0.5 V potential in the absence or in the presence of 5×10^{-5} M to 3×10^{-4} M Fe^{3+} using 9.5 cm² cathode surface area and 0.05 M $NaClO_4$ as supporting electrolyte. The change of AB9 decolorization with time is depicted in Fig. 8. It can be observed that in the absence of Fe^{3+}, about 23% of AB9 is destructed at 120 min. It can be attributed to direct reaction of dye with H_2O_2 or its reaction with $^\bullet$OH formed from anodic oxidation process. Decolorization efficiency undergoes a fast acceleration when Fe^{3+} is added. Fe^{3+} react with H_2O_2 (Eq. (8)) and produce $HO_2^\bullet$ and Fe^{2+} from Fenton-like process. Regenerated Fe^{2+} can react with H_2O_2 and produce strong hydroxyl radicals. In addition, Fe^{2+} can be regenerated at cathode surface from reduction of Fe^{3+} (Eq. (10)) [45]. By increasing Fe^{3+} concentration to 10^{-4} M, AB9 decay increases. This effect can be related to both increasing $HO_2^\bullet$ concentration (Eq. (8)) and also an increasing quantity of Fe^{2+} regenerated (Eqs. (8) and (10)) which subsequently enhance the production of strong oxidant $^\bullet$OH by Fenton's reaction (Eq. (11)). However, at higher Fe^{3+} concen-
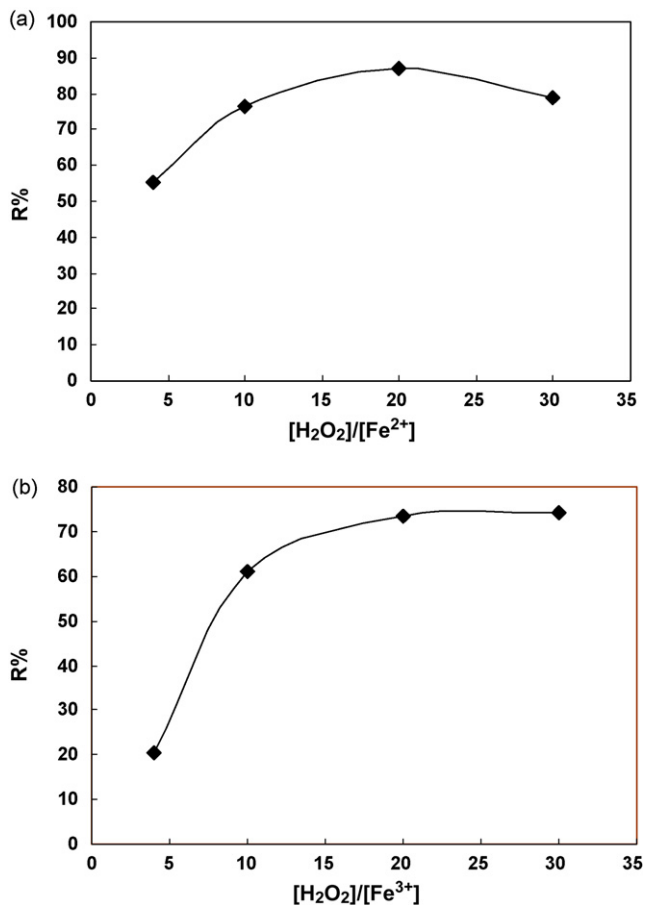
Fig. 6. Effect of ratio of [H_2O_2]/[Fe ion] on AB9 decolorization; pH 3.0, $C_0 = 20$ mg/l, and stirring speed = 200 rpm. (a) Fenton process (Fe^{2+}, after 2 min); (b) Fenton-like process (Fe^{3+}, after 40 min).

tration, effect of increasing ferric concentration on decolorization efficiency is negligible. In fact, before optimum concentration of Fe^{3+} (10^{-4} M), Fe^{3+} concentration is rate-determining and controls the overall reaction rate. However, after 10^{-4} M Fe^{3+}, H_2O_2 concentration is limiting parameter and therefore, although Fe^{3+} concentration increases, production of $^{\bullet}$OH is constant. These findings concludes that a small concentration of Fe^{3+} is effective for electro-Fenton systems.
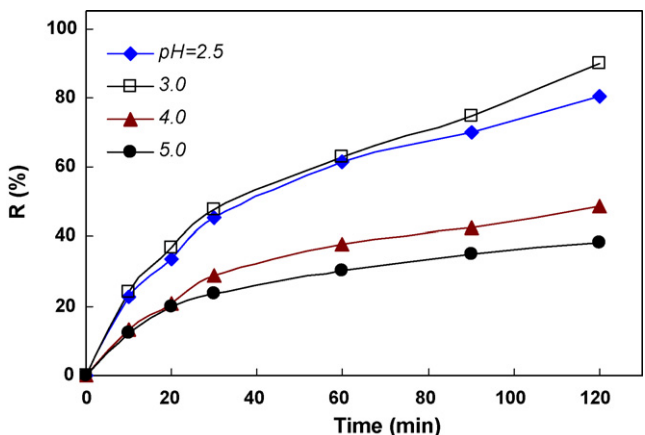

Fig. 7. Decolorization of AB9 in different pH solutions by electro-Fenton application; $C_0 = 20$ mg/l, [NaClO$_4$] = 0.05 M, $A = 9.5$ cm^2, $E = -0.5$ V, and stirring speed = 200 rpm.
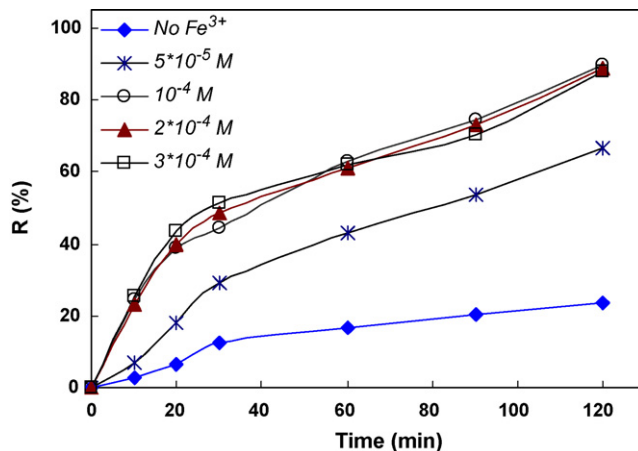

Fig. 8. Effect of Fe^{3+} concentration on decolorization of AB9 by electro-Fenton process; $C_0 = 20$ mg/l, [NaClO$_4$] = 0.05 M, pH 3.0, $A = 9.5$ cm^2, $E = -0.5$ V, and stirring speed = 200 rpm.
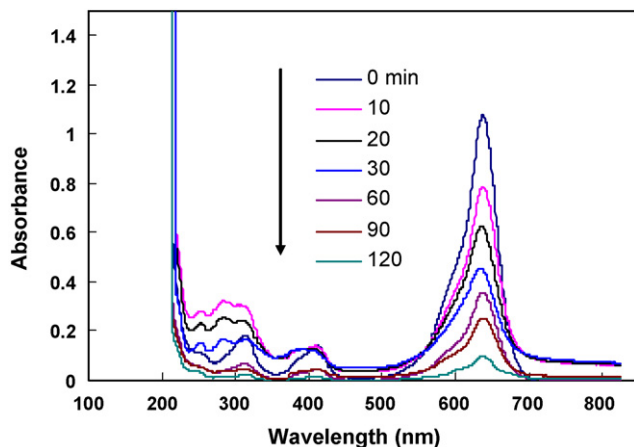

Fig. 9. UV–vis spectra changes of AB9 (20 mg/l) by electro-Fenton process; [NaClO$_4$] = 0.05 M, pH 3.0, $A = 9.5$ cm^2, $E = -0.5$ V, and stirring speed = 200 rpm.
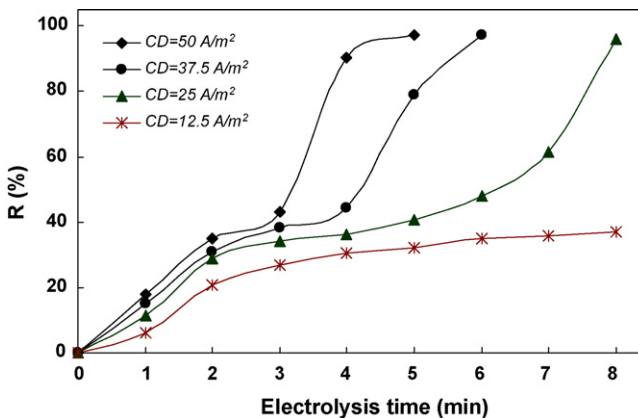

Fig. 10. Variation of color removal efficiency with time at different current densities; $C_0 = 20$ mg/l, pH 6.08, $\gamma = 15.9$ mS/cm, and stirring speed = 200 rpm.

Fig. 9 shows time-dependent UV–vis spectrum of AB9 solution during electro-Fenton process. As it is clear from this figure, the absorption peaks diminished and finally disappeared under reaction, which indicated that the AB9 had been degraded. No new absorption bands appear in either the visible or ultraviolet regions.
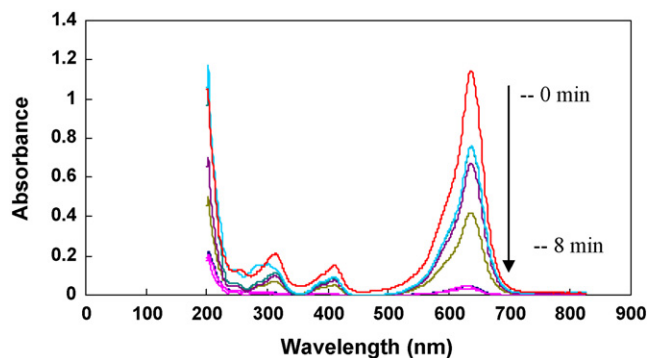
Fig. 11. UV–vis spectra changes of C.I. Acid Blue 9 at various electrolysis times; CD = 25 A/m^2, C_0 = 20 mg/l, pH 6.08, γ = 15.9 mS/cm, and stirring speed = 200 rpm.
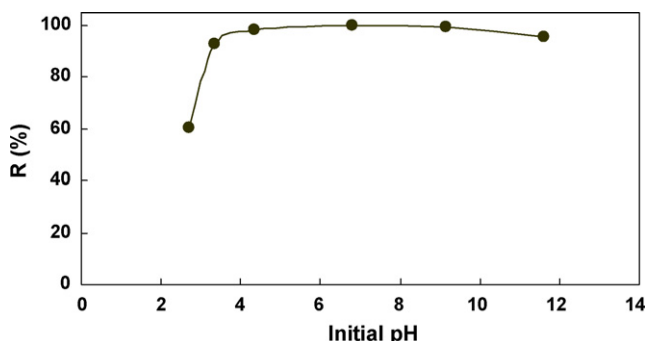

Fig. 12. Effect of initial pH on the color removal efficiency; CD = 25 A/m^2, t_{EC} = 8 min, C_0 = 20 mg/l, γ = 15.9 mS/cm, and stirring speed = 200 rpm.

3.4. Decolorization efficiency of electrocoagulation process

In this section the efficiency of EC process on decolorization of the dye solution containing 20 mg/l AB9 was evaluated by iron electrode. According to the pervious works [33], at the same concentration of pollutant the current density, electrolysis time and pH are the most effective parameters that affect color removal efficiency in the EC process.

According to Faraday's formula (Eq. (22)), it is clear that Fe^{2+} dose released from anode depends on the electrolysis time and current. So in the electrocoagulation process, current (I) and electrolysis time (t) are the most important parameters affecting the color removal efficiency and controlling the reaction rate in the reactor.
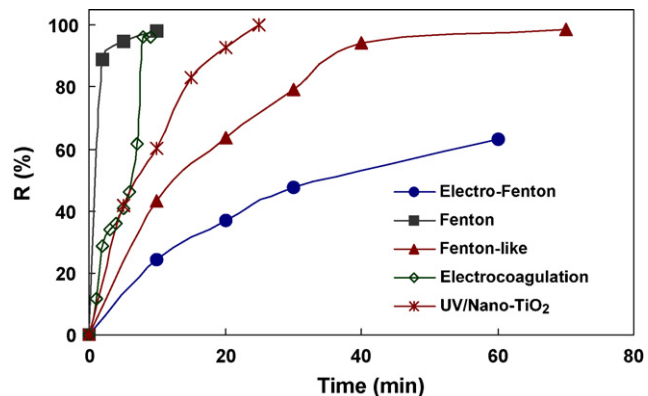

Fig. 13. Comparison of different AOPs and EC method on decolorization of 20 mg/l AB9.

Table 2
The electrical energy required to complete decolorization (R > 95%) of solution containing 20 mg/l AB9 (pH 6.08) at various current densities by electrocoagulation method

Current (A)	Current density (A/m^2)	Required time (min)	Energy consumption (kWh/m^3)
0.05	12.5	16	0.058
0.10	25	8	0.074
0.15	37.5	6	0.102
0.20	50	5	0.140

$$C_{Fe} = \frac{M_w I t_{EC}}{ZFV} \qquad (22)$$

where C_{Fe}, Z, F, V, and M_w are the theoretical concentration of Fe^{2+} (g/m^3), the chemical equivalence, Faraday constant (96,487 C/mol), volume of reactor (m^3), and molecular weight of iron (g/mol), respectively [35]. Fig. 10 shows the electrolysis time versus the color removal efficiency at different CDs. As it can be seen, when current density and/or electrolysis time raises, the color removal efficiency is improved. It appeared that at lower current densities, the less iron was released from the anode and hence the color removal efficiency was low. When the current density increased significant amount of flocs generated, which in turn trapped the dye molecules and enhanced the color removal efficiency (Fig. 10). The color removal efficiency increased to 97.26% at 50 A/m^2 from 35.24% at 12.5 A/m^2 at the electrolysis time of 8 min.

The changes in the absorption spectra of AB9 solution during the EC process at different electrolysis times are shown in Fig. 11. The spectrum of AB9 in the visible region exhibits a main band with a maximum at 625 nm. This figure shows the absorption peaks corresponding to dye molecules diminish and finally disappear with increase of the reaction time.

It is clear that a technically efficient process must also be feasible economically. The major operating cost of EC is associated with electrical energy consumption during process. Although increasing current density and electrolysis time enhances the efficiency of EC, it causes to raise the cell voltage, energy consumption and operating costs consequently. The electrical energy required to decolorization (R > 95%) of the solution containing 20 mg/l AB9 at various current densities was calculated in terms of kWh/m^3 using the equation given as follows:

$$E = \frac{U I t_{EC}}{V_s} \times 10^{-3} \qquad (23)$$

where U is the voltage measured during the reaction (V), I the applied electrical current (A), t_{EC} the electrolysis time (h), and V_s the volume of dye solution (m^3). According to the results presented in Table 2, for a solution with the dye concentration of 20 mg/l, the suitable current density and electrolysis time were 25 A/m^2 and 8 min, respectively.

The EC process is highly dependent on the initial pH of the solution [32]. The experiments were carried out at pH 2–11.8 with 20 mg/l AB9 solution. The current density was maintained at 25 A/m^2. The color removal efficiency as a function of initial pH of the dye solution is shown in Fig. 12. It can be seen that the initial pH has significant effect on the color removal efficiency especially at low pH. The results indicated that the color removal efficiency increased with increase of pH and it remained unchanged between pH 4.5 and 9 and then on further increase of pH, the color removal efficiency decreased. Therefore, it can be concluded that at pH range of 4.5–9, the majority of iron complexes (coagulants) are formed and it is the optimum pH for carrying out the electrocoagulation. There was minimum color removal efficiency at pH < 2.5, because at this pH, hydroxide ions generated at the cathode neutralized with H$^+$ ions and sufficient amount of iron hydroxide complexes did

Table 3
Kinetic constants and electrical energy consumption for decolorization of 20 mg/l AB9 using different processes

Process	Kinetic model	Rate constant	R^2	$t_{1/2}$ (min)	Electrical energy consumption (kWh/m^3)
UV/Nano-TiO$_2$	First order	0.1141 min^{-1}	0.973	6.073	175.44
Fenton	Second order	0.615 min^{-1} M^{-1}	0.934	0.267	–
Fenton-like	First order	0.0233 min^{-1}	0.984	29.74	–
Electro-Fenton	First order	0.0108 min^{-1}	0.988	64.18	300
Electrocoagulation	First order	0.1206 min^{-1}	0.928	5.72	0.074

not form. At the pH > 9 color removal efficiency decreased about 9%, because above this pH, Fe(OH)$_4^-$ was the dominant species which was a dissolving species and it was unable to form flocs [32].

3.5. Comparison of the color removal efficiencies of different AOPs and EC methods

The comparison of different AOPs and electrochemical method is of interest to determine the best color removal performance and the most efficient process for the removal of target compound in the dye solution. The efficiency of decolorization of AB9 solution by different AOPs and electrochemical methods are illustrated in Fig. 13. It can be seen that the most effective AB9 decolorization rate was obtained by Fenton process and the ranking was in the order of Fenton > EC > UV/Nano-TiO$_2$ > Fenton-like > EF. In addition, the kinetic model, kinetic rate constant and electrical energy consumption have been compared in Table 3. According to these results, it is clear that the rate constant of Fenton process was higher than other processes (Table 3). However, selectivity of the suitable process for treatment of pollutants is related to various conditions such as economical aspects, required equipments, operational problems, secondary pollutions, energy consumption, etc. For example, although electrocoagulation is an effective method for removal of AB9 in the term of decolorization efficiency and electrical energy consumption (Table 3), it is not destructive and only transfers the contamination from one phase (aqueous) to another phase (flocs). The advantages of photocatalysis are: destructive, no sludge production, potential of solar light utilization. But, light penetration limitation, fouling of the photocatalyst, and problem of fine TiO$_2$ separation from the treated liquid in slurry reactors are some of the disadvantages of this method. Fenton process is effective within narrow pH range of <3.5; and involves sludge generation. Electro-Fenton process requires further development for industrial acceptance. High cost of electricity is an impediment. It also comparatively required longer reaction time.

4. Conclusion

In this study, we assessed the possibility of different AOPs and electrocoagulation method for the AB9 decolorization. The following conclusions can be drawn from this work:

- The results indicated that the photocatalytic degradation of AB9 were obviously affected by the initial pH and the amount of TiO$_2$ nanoparticles. We learned that the desired amount of the photocatalyst was 150 ppm, with AB9 concentration of 20 ppm. It was also found that the best photocatalytic activity was obtained in acidic condition.
- The desired H$_2$O$_2$ dose and iron ion concentration for Fenton and for Fenton-like was found to be 2×10^{-3} M and 10^{-4} M, respectively.
- Decolorization was faster using Fenton oxidation process, whereas the electro-Fenton process was slower method. However, electro-Fenton process generated H$_2$O$_2$ in situ.

- Electrocoagulation is an effective method for removal of AB9 in terms of decolorization efficiency, but it is not destructive and only transfers the contamination from aqueous phase to sludge. Decolorization of AB9 solution by electrocoagulation was affected by the current density, time of electrolysis and initial pH of the dye solution. It was found that for a solution with dye concentration of 20 mg/l, decolorization efficiency was of 98%, when the pH was about 6, time of electrolysis was 8 min and current density was approximately 25 A/m^2.
- It was found that the ranking of AB9 decolorization efficiency was in the order of Fenton > EC > UV/Nano-TiO$_2$ > Fenton-like > EF.

References

[1] Y. Anjaneyulu, N. Sreedhara Chary, D. Samuel Suman Raj, Decolourization of industrial effluents—available methods and emerging technologies—a review, Rev. Environ. Sci. Biotechnol. 4 (2005) 245–273.
[2] N. Azbar, T. Yonar, K. Kestioglu, Comparison of various advanced oxidation processes and chemical treatment methods for COD and color removal from a polyester and acetate fiber dyeing effluent, Chemosphere 55 (2004) 35–43.
[3] A. Wang, J. Qu, J. Ru, H. Liu, J. Ge, Mineralization of an azo dye acid red 14 by electro-Fenton's reagent using an activated carbon fiber cathode, Dyes Pigments 65 (2005) 227–233.
[4] C. Galindo, P. Jacques, A. Kalt, Photochemical and photocatalytic degradation of an indigolid dye: a case study of acid blue 74 (AB74), J. Photochem. Photobiol. A 141 (2001) 47–56.
[5] J.H. Oliver, K. Hyunook, C. Pen-Chi, Decolorization of wastewater, Crit. Rev. Environ. Sci. Technol. 30 (4) (2000) 499–505.
[6] C. Walling, Fenton's reagent revisited, Acc. Chem. Res. 8 (1975) 125–131.
[7] J.J. Pignatello, Dark and photoassisted Fe^{3+}-catalyzed degradation of chlorophenoxy herbicides by hydrogen peroxide, Environ. Sci. Technol. 26 (1992) 944–951.
[8] E. Brillas, J.C. Calpe, J. Casado, Mineralization of 2,4-D by advanced electrochemical oxidation processes, Water Res. 34 (2000) 2253–2262.
[9] G.F. Ijpelaar, R.T. Meijers, R. Hopman, J.C. Kruithof, Ozone Sci. Eng. 22 (2000) 607.
[10] F. Chen, J. He, J. Zhao, J.C. Yu, Photo-Fenton degradation of malachite green catalyzed by aromatic compounds under visible light irradiation, New J. Chem. 26 (2002) 336–341.
[11] N. Daneshvar, A.R. Khataee, Removal of azo dye C.I. acid red 14 from contaminated water using Fenton, UV/H$_2$O$_2$, UV/H$_2$O$_2$/Fe(II), UV/H$_2$O$_2$/Fe(III) and UV/H$_2$O$_2$/Fe(III)/oxalate processes: a comparative study, J. Environ. Sci. Health A 41 (3) (2006) 315–328.
[12] A. Mohey El-Dein, J.A. Libra, U. Wiesmann, Mechanism and kinetic model for the decolorization of the azo dye reactive black 5 by hydrogen peroxide and UV radiation, Chemosphere 52 (2003) 1069–1077.
[13] G.R. Peyton, W.H. Glaze, Destruction of pollutants in water with ozone in combination with ultraviolet radiation. 3. Photolysis of aqueous ozone, Environ. Sci. Technol. 22 (1988) 761–767.
[14] C. Flox, S. Ammar, C. Arias, E. Brillas, A.V. Vargas-Zavala, R. Abdelhedi, Electro-Fenton and photoelectro-Fenton degradation of indigo carmine in acidic aqueous medium, Appl. Catal. B 67 (2006) 93–104.
[15] N. Daneshvar, D. Salari, A.R. Khataee, Photocatalytic degradation of azo dye acid red 14 in water: investigation of the effect of operational parameters, J. Photochem. Photobiol. A 157 (2003) 111–116.
[16] N. Daneshvar, A.R. Khataee, D. Salari, A. Niaie, M.H. Rasoulifard, Immobilization of TiO$_2$ nanopowder on glass beads for the photocatalytic decolorization of an azo dye C.I. direct red 23, J. Environ. Sci. Health A 40 (2005) 1605–1617.
[17] E. Piera, J.C. Calpe, E. Brillas, X. Domènech, J. Peral, 2,4-Dichlorophenoxyacetic acid degradation by catalyzed ozonation: TiO$_2$/UVA/O$_3$ and Fe(II)/UVA/O$_3$ systems, Appl. Catal. B 27 (2000) 169–177.

[18] N. Daneshvar, A.R. Khataee, M.H. Rasoulifard, F. Hosseinzadeh, Removal of C.I. acid orange 7 from aqueous solution by UV irradiation in the presence of ZnO nanopowder, J. Hazard. Mater. 143 (2007) 95–101.

[19] N. Daneshvar, A.R. Khataee, D. Salari, Photocatalytic degradation of azo dye acid red 14 in water on ZnO as an alternative catalyst to TiO_2, J. Photochem. Photobiol. A 162 (2004) 317–322.

[20] A. Fujishima, A.X. Zhang, Titanium dioxide photocatalysis: present situation and future approaches, C. R. Chim. 9 (2006) 750–760.

[21] M. Ni, M.K.H. Leung, D.Y.C. Leung, K. Sumathy, A review and recent developments in photocatalytic water-splitting using TiO_2 for hydrogen production, Renew. Sustain. Energy Rev. 11 (2007) 401–425.

[22] K. Pirkanniemi, M. Sillanpaa, Heterogeneous water phase catalysis as an environmental application: a review, Chemosphere 48 (2002) 1047–1060.

[23] T. Yates Jr., T.L. Thompson, Surface science studies of the photoactivation of TiO_2-new photochemical processes, Chem. Rev. 106 (2006) 4428–4453.

[24] A. Fujishima, T.N. Rao, D.A. Tryk, Titanium dioxide photocatalysis, J. Photochem. Photobiol. C 1 (2000) 1–21.

[25] B. Ensing, F. Buda, E.J. Baerends, Fenton-like chemistry in water: oxidation catalysis by Fe(III) and H_2O_2, J. Phys. Chem. 107(A) (2003) 5722–5731.

[26] B. Boye, M.M. Dieng, E. Brillas, Anodic oxidation, electro-Fenton and photoelectro-Fenton treatments of 2,4,5-trichlorophenoxyacetic acid, J. Electroanal. Chem. 557 (2003) 135–146.

[27] M. Panizza, G. Cerisola, Removal of organic pollutants from industrial wastewater by electrogenerated Fenton's reagent, Water Res. 35 (2001) 3987–3992.

[28] E. Guivarch, S. Trevin, C. Lahitte, M.A. Oturan, Degradation of azo dyes in water by electro-Fenton process, Environ. Chem. Lett. 1 (2003) 38–44.

[29] M. Diagne, N. Oturan, M.A. Oturan, Removal of methyl parathion from water by electrochemically generated Fenton's reagent, Chemosphere 66 (2007) 841–848.

[30] M. Kobya, O.T. Can, M. Bayramoglu, Treatment of textile wastewaters by electrocoagulation using iron and aluminum electrodes, J. Hazard. Mater. B 100 (2003) 163–178.

[31] M.Y.A. Mollah, S.R. Pathak, P.K. Patil, M. Vayuvegula, T.S. Agrawal, J.A.G. Gomes, M. Kesmez, D.L. Cocke, Treatment of orange II azo-dye by electrocoagulation (EC) technique in a continuous flow cell using sacrificial iron electrodes, J. Hazard. Mater. B 109 (2004) 165–171.

[32] M.Y.A. Mollah, P. Morkovsky, J.A.G. Gomes, M. Kesmez, J. Parga, D.L. Cockec, Fundamentals, present and future perspectives of electrocoagulation, J. Hazard. Mater. B 114 (2004) 199–210.

[33] N. Daneshvar, A.R. Khataee, A.R. Amani Ghadim, M.H. Rasoulifard, Decolorization of C.I. acid yellow 23 solution by electrocoagulation process: investigation of operational parameters and evaluation of specific electrical energy consumption (SEEC), J. Hazard. Mater. B 148 (2007) 566–572.

[34] P. Cañizares, M. Carmona, J. Lobato, F. Martinez, M.A. Rodrigo, Electrodissolution of aluminum electrodes in electrocoagulation processes, Ind. Eng. Chem. Res. 44 (2005) 4178–4185.

[35] N. Daneshvar, A. Oladegaragoze, N. Djafarzadeh, Decolorization of basic dye solutions by electrocoagulation: an investigation of the effect of operational parameters, J. Hazard. Mater. B 129 (2006) 116–122.

[36] A.R. Khataee, N. Daneshvar, D. Salari, A. Niaei, Photocatalytic degradation of the herbicide erioglaucine in the presence of nanosized titanium dioxide: comparison and modeling of reaction kinetics, J. Environ. Sci. Health B 41 (2006) 1273–1290.

[37] N. Daneshvar, S. Aber, V. Vatanpour, M.H. Rasoulifard, Electro-Fenton treatment of dye solution containing orange.II. Influence of operational parameters, J. Electroanal. Chem. 615 (2008) 165–174.

[38] A.L. Linsebigler, G. Lu, J.T. Yates Jr., Photocatalysis on TiO_2 surfaces: principles, mechanisms, and selected results, Chem. Rev. 95 (1995) 735–758.

[39] U. Diebold, The surface science of titanium dioxide, Surf. Sci. Rep. 48 (2003) 53–229.

[40] R.F.P.M. Moreira, T. Sauer, G. Cesconeto, H.J. Jose, Kinetics of photocatalytic degradation of reactive dyes in a TiO_2 slurry reactor, J. Photochem. Photobiol. A 149 (2002) 147–154.

[41] M.S.T. Goncalves, A.M.F. Oliveira-Campos, E.M.M.S. Pinto, P.M.S. Plasencia, M.J.R.P. Queiroz, Photochemical treatment of solutions of azo dyes containing TiO_2, Chemosphere 39 (1999) 781–786.

[42] M.S. Lucas, J.A. Peres, Decolorization of the azo dye reactive black 5 by Fenton and photo-Fenton oxidation, Dyes Pigments 71 (2006) 236–244.

[43] Z. Qiang, J.-H. Chang, C.P. Huang, Electrochemical generation of hydrogen peroxide from dissolved oxygen in acidic solutions, Water Res. 36 (2002) 85–94.

[44] I. Sirés, C. Arias, P.L. Cabot, F. Centellas, J.A. Garrido, R.M. Rodríguez, E. Brillas, Degradation of clofibric acid in acidic aqueous medium by electro-Fenton and photoelectro-Fenton, Chemosphere 66 (2007) 1660–1669.

[45] I. Sirés, J.A. Garrido, R.M. Rodríguez, E. Brillas, N. Oturan, M.A. Oturan, Catalytic behavior of the Fe^{3+}/Fe^{2+} system in the electro-Fenton degradation of the antimicrobial chlorophene, Appl. Catal. B 72 (2007) 382–394.